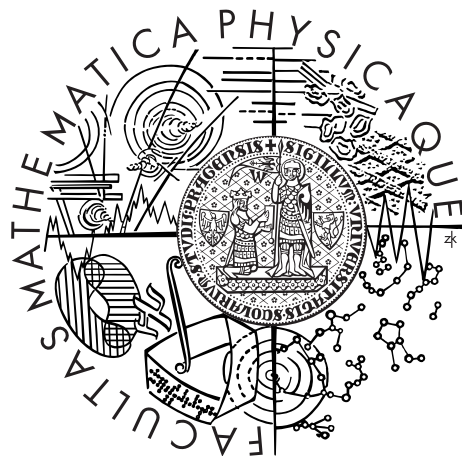


Charles University in Prague  
Faculty of Mathematics and Physics

## MASTER THESIS



Martin Pecka

# Detection of 2D features in MARSIS ionogram pictures

Department of Software Engineering 

Supervisor of the master thesis: RNDr. Jana Štanclová, Ph.D.

Study programme: Informatics

Specialization: Theoretical Informatics

Prague 2013

Dedication.

I declare that I carried out this master thesis independently, and only with the cited sources, literature and other professional sources.

I understand that my work relates to the rights and obligations under the Act No. 121/2000 Coll., the Copyright Act, as amended, in particular the fact that the Charles University in Prague has the right to conclude a license agreement on the use of this work as a school work pursuant to Section 60 paragraph 1 of the Copyright Act.

In Prague date .....

Název práce: Hledání 2D jevů v ionografických snímcích přístroje MARSIS

Autor: Bc. Martin Pecka

Ústav: Ústav výpočetní techniky Univerzity Karlovy v Praze

Vedoucí diplomové práce: RNDr. Jana Štanclová, Ph.D.,  
Ústav výpočetní techniky Univerzity Karlovy v Praze

**Abstrakt:** Práce se zabývá technikami hledání význačných prvků v ionogramech zachycených přístrojem MARSIS umístěným na kosmické sondě Mars Express. Identifikace těchto prvků pomáhá při studiu ionosféry, magnetosféry a plazmatu v okolí Marsu. Ionogramy jsou reprezentovány jako dvourozměrné obrázky s hodnotou kódovanou pomocí barvy. Cílem práce je navrhnout techniky pro detekci různých zajímavých křivek (definovaných sadou parametrů) v ionogramech, případně pro měření dalších parametrů nalezených objektů (perioda opakování přímek).

**Klíčová slova:** rozpoznávání vzorů, detekce objektů, parametrické křivky, Mars Express, vektorizace

Title: Detection of 2D features in MARSIS ionogram pictures

Author: Bc. Martin Pecka

Centre: Charles University Computer Centre

Supervisor: RNDr. Jana Štanclová, Ph.D., Charles University Computer Centre

**Abstract:** The work focuses on techniques for finding significant features in ionograms captured by the MARSIS instrument onboard the Mars Express spacecraft. Identification of these features helps in studying the ionosphere, magnetosphere and plasma surrounding Mars. Ionograms are 2D images with values represented in color. The goal of this work is to propose techniques to detect interesting curves (parametrically defined) in such images and to measure some more parameters of the found objects (like the repetition period of lines).

**Keywords:** pattern recognition, object detection, parametric curves, Mars Express, vectorization

# Contents

<b>Introduction</b>	<b>3</b>
<b>1 Mars Express, MARSIS and ionograms</b>	<b>4</b>
1.1 Mars Express . . . . .	4
1.1.1 High-Resolution Stereo Camera (HRSC) . . . . .	5
1.1.2 Observatoire pour la Minéralogie, l'Eau, les Glaces et l'Activité (OMEGA) . . . . .	7
1.1.3 Mars Advanced Radar for Subsurface and Ionosphere Sounding (MARSIS) . . . . .	7
1.1.4 Planetary Fourier Spectrometer (PFS) . . . . .	8
1.1.5 SPectroscopy for the Investigation of the Characteristics of the Atmosphere of Mars (SPICAM) . . . . .	9
1.1.6 Analyser of Space Plasmas and EneRgetic Atoms (ASPERA-3) . . . . .	10
1.1.7 Mars Express Orbiter Radio Science (MaRS) . . . . .	11
1.1.8 Beagle 2 . . . . .	12
1.2 The MARSIS experiment . . . . .	13
1.2.1 Subsurface sounding . . . . .	13
1.2.2 Surface sounding . . . . .	14
1.2.3 Ionospheric sounding . . . . .	14
1.3 Ionograms . . . . .	15
1.3.1 Ionospheric echo . . . . .	16
1.3.2 Surface echo . . . . .	17
1.3.3 Oblique ionospheric echo . . . . .	17
1.3.4 Electron plasma oscillation harmonics . . . . .	19
1.3.5 Electron cyclotron echoes . . . . .	19
<b>2 The detection problem</b>	<b>21</b>
2.1 Definition . . . . .	21
2.1.1 Ionogram . . . . .	21
2.1.2 Features to detect . . . . .	22
2.2 Title of the second subchapter of the second chapter . . . . .	24
<b>Conclusion</b>	<b>26</b>
<b>Bibliography</b>	<b>27</b>
<b>List of Tables</b>	<b>31</b>

**List of Abbreviations** **32**

**Attachments** **33**

# Introduction

# 1 Mars Express, MARSIS and ionograms

In this chapter we introduce the Mars Express spacecraft and its scientific payload. We describe all the appliances, their goals and successes so far. In the second section we present the MARSIS instrument in detail showing the principles of its experiments. The last part of this chapter is devoted to the description of ionograms – a specific visualization of the ionospheric sounding data from MARSIS.

## 1.1 Mars Express

First of all, we briefly introduce the spacecraft carrying all the equipment needed to acquire ionograms. Its name is Mars Express (MEX) and it was launched by the European Space Agency (ESA) on 2 June 2003. A visualization of the spacecraft is provided in Fig. 1.1.

MEX arrived to Mars at its orbit with periapsis 250 km and apoapsis over 11,000 km on 25 December 2003 [12] with seven onboard scientific instruments and a landing module called Beagle 2. Unfortunately, the landing sequence of Beagle 2 failed (for an unknown reason) and the lander did not establish connection after it landed (if it landed at all)[12, p. 4].

The mission of MEX has several goals like “global studies of the surface, subsurface and atmosphere at unprecedented spatial and spectral resolutions” [12, p. viii]. One of the goals, however, stands out among all the others. It is the search for water (or its traces) on martian surface or subsurface.

There is lots of geological evidence of former water occurrence on Mars [12, p. ix]. But before the MEX mission nobody had proved or refuted presence of water on Mars in the present. Knowing more about water on Mars and its history, the scientists could postulate better hypotheses about the possibility of (former) life on the planet [12, p. ix].

The original mission lifetime of MEX was projected up to the end of 2005 (which would be 1 Martian year = 687 Earth days) [13]. During its lifetime, MEX encountered some small problems<sup>1</sup>. Nevertheless, it has worked on its science goals up to this day and its science mission was extended until 2014 [19] (after 3 preceding similar extensions). According to Fred Jansen, MEX mission manager, MEX had enough fuel for another 14 years of operation (at the beginning of 2012) [9]. So there is a hopeful prospect of further and even

---

<sup>1</sup>as the Solid State Mass Memory anomalies described in [17] or the MARSIS antennas deployment problems in 2004 [14, 15]

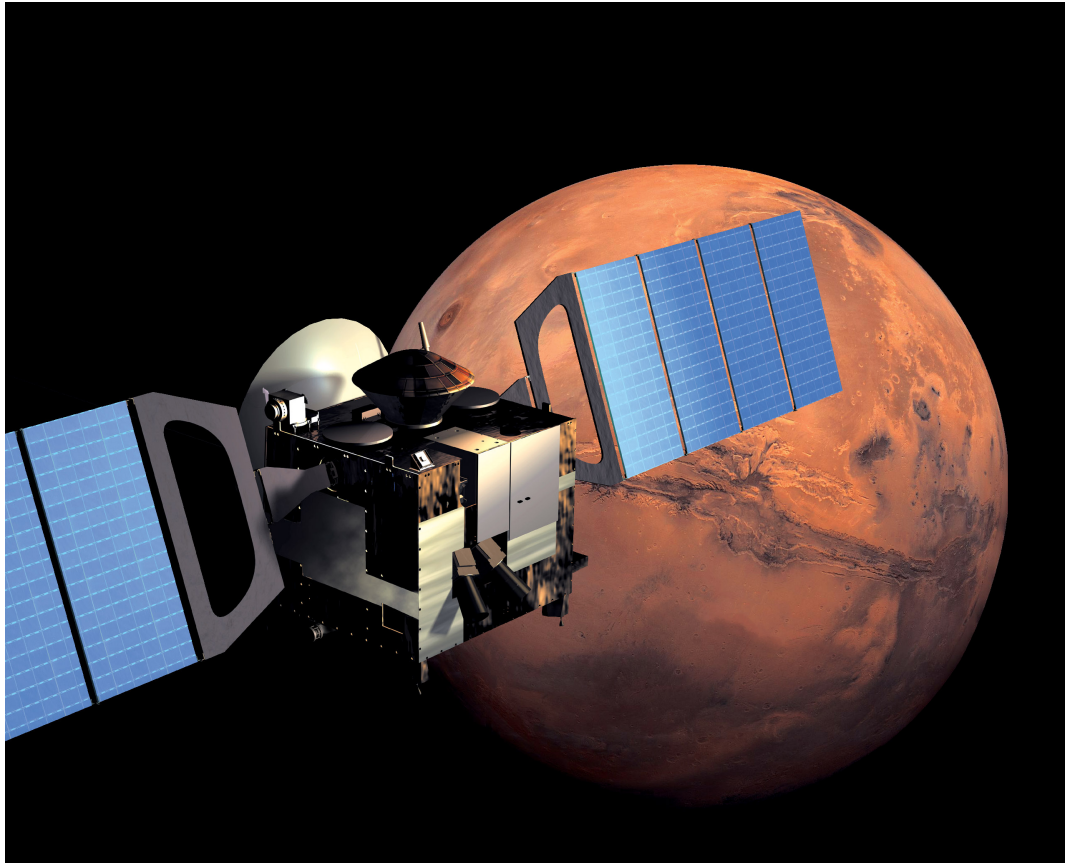


Figure 1.1: Mars Express spacecraft. [16]

deeper Mars exploration (e.g. like the discovery of an unexpected way of using the MARSIS instrument which “added magnetometer functionality” to MARSIS [21]).

In the next subsections particular MEX instruments are described. The descriptions are based on [12] which can be consulted for more detailed information.

### 1.1.1 High-Resolution Stereo Camera (HRSC)

HRSC is a high-resolution pushbroom<sup>2</sup> camera for surface imaging. Its goals are: [12, p. 17]

- to characterize surface structure and morphology at resolution  $10 \text{ m.px}^{-1}$  (regions of interest at  $2 \text{ m.px}^{-1}$ )
- to record surface topology at high vertical resolution
- to observe atmospheric phenomena
- to analyze physical properties of the surface

---

<sup>2</sup>A camera that scans the image by rows perpendicular to the flight direction. See [http://earthobservatory.nasa.gov/Features/E01/e01\\_2.php](http://earthobservatory.nasa.gov/Features/E01/e01_2.php) for more details.

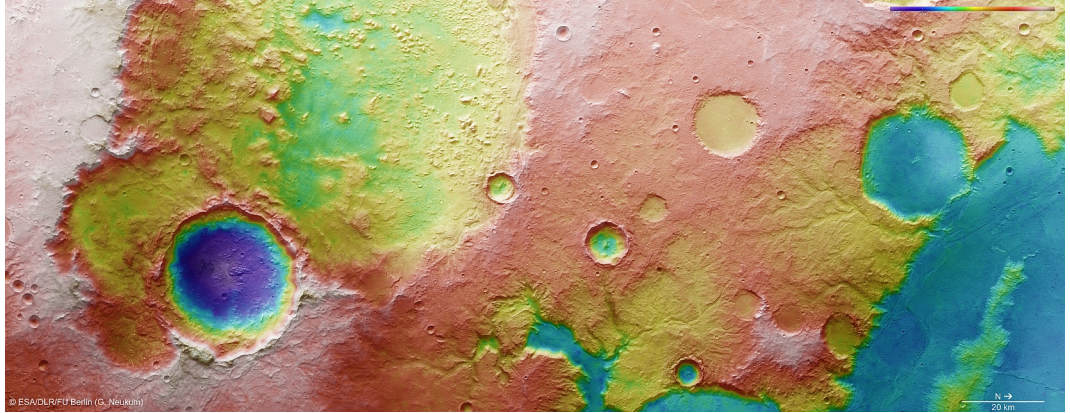


Figure 1.2: Example image taken by HRSC. [28]

- to classify terrain and thus refine the martian cartographic base
- to observe martian moons Phobos and Deimos during their approaches

HRSC is able to capture the surface at resolution up to  $10 \text{ m.px}^{-1}$  with field of view  $11.9^\circ$ , covering a 52.2 km wide strip of surface at height 250 km (which is the periapsis of MEX). The camera consists of 9 CCD (Charge-coupled device) sensors allowing it to acquire triple stereo images in 4 colors and 5 phase angles. A very useful property of these images is that they are taken nearly simultaneously and thus have the same illumination and other observational conditions (which further helps in photogrammetric processing of the images) [12, pp. 24–30].

In addition to the stereo camera, the instrument also contains a super-high-resolution camera called SRC (Super-Resolution Channel) aimed at targeted observations of particular surface details. With image resolution  $2.3 \text{ m.px}^{-1}$  and field of view  $0.54^\circ$  it provides a detailed view of a  $2.3 \times 2.35 \text{ km}$  large surface. Its main purpose is to take details of places of interest, e.g. future landing sites for other landing modules [12, p. 28].

Up to November 2011 HRSC had covered about 88 % of the martian surface [18, pp. 72–73] and still continues to gather new data. An example photograph from HRSC is given in Fig. 1.2. The scientific results of HRSC are for example:

- better exploration of fluvial valleys [25]
- discovery of numerous glacial landforms [20, p. 5]
- investigating lava flows [20, p. 28]
- discovery of “dust devils” (fast moving dust storms) [20, p. 47]
- providing data to derive a detailed topographic model of more than 20 % of Phobos [22, pp. 945–949]

### **1.1.2 Observatoire pour la Minéralogie, l'Eau, les Glaces et l'Activité (OMEGA)**

OMEGA is a medium- and high-resolution spectrometer operating in visible and near-infrared (near-IR) spectra ( $0.38\text{--}5.1\,\mu\text{m}$  wavelength). Its medium-resolution operating mode (from heights of 1,500 to 4,000 km) can measure with the resolution 2–5 km targeting at global surface coverage. In the high-resolution mode (from the close vicinity of periapsis) it achieves resolution 350 m or better, but can cover only a small fraction of the surface [12, p. 37].

As stated in [12, pp. 38–39], the main goals of OMEGA are:

- to study the evolution of Mars
- to detect minerals hidden to lower resolutions
- to map mineralogical boundaries between geological units
- to reveal gradients in hydration minerals related to fossil water flows
- to monitor features associated with wind transportation

In particular, OMEGA is intended to find carbonates (not found on martian surface until the launch of MEX) and water ice. It is also able to measure atmospheric pressure, CO and H<sub>2</sub>O column densities and surface temperature.

Recent contributions of the OMEGA payload are e.g.:

- confirmation of liquid water on the surface when the planet was young [23]
- discovery of IR and ultraviolet (UV) glows in the atmosphere [4]
- proving that Mars had a hot and wet period [7] (implying there were lots of greenhouse gases and a strong magnetic field, too [20, p. 90])
- analyzing the south polar cap and finding out it is formed mainly of water ice [10]
- observation of CO<sub>2</sub> ice clouds [27]
- finding ferric oxides near the equator [26]

### **1.1.3 Mars Advanced Radar for Subsurface and Ionosphere Sounding (MARSIS)**

MARSIS is a long-wavelength radar using coherent wide-band pulses for sounding of the surface, subsurface and ionosphere of Mars. For these purposes it uses a 40 m dipole antenna (for both transmitting and receiving) and a shorter 7 m

monopole antenna (only for receiving). Due to the used sounding frequencies ranging from 100 kHz to 5.5 MHz it is able to reach the depth about 5–8 km under the surface [12, pp. 51, 57].

The primary goal of MARSIS is to detect liquid and solid water in the upper crust of Mars. There are also other objectives: [12, p. 51]

- subsurface geologic probing (to make a 3D characterization of the subsurface structures)
- surface characterization (to measure surface roughness, reflectance to radar signals and to estimate topography)
- ionosphere sounding (to measure interaction between solar wind and the ionosphere)

To name some results of the MARSIS instrument, we can mention the following:

- revealing the layered subsurface structure of both polar caps (strongly suggesting there were oceans in distant history at these places) [20, pp. 98–102]
- estimating the volume of subsurface water ice in the polar cap [30]
- discovery of Medusae Fossae Formations (the youngest surface deposits) [20, pp. 102–105]
- mapping the ionosphere and verifying the ionospheric density models [20, pp. 105–110]

One surprising and unexpected utilization of the MARSIS instrument is given by the electron cyclotron echoes found in ionograms (see section 1.3.5). It was found that the echoes often correspond to the strength of the magnetic field, effectively allowing to measure that field and compare it to its model. Another type of echoes, the oblique ionospheric echoes (see section 1.3.3) were identified to correspond to the crustal magnetic field. Both these contributions were made by [21].

#### 1.1.4 Planetary Fourier Spectrometer (PFS)

PFS is IR-spectrometer (based on double-pendulum interferometer) operating in the range 1.2–42  $\mu\text{m}$  divided into two channels – the Short Wavelength (SW) channel (1.2–5  $\mu\text{m}$ ) and the Long Wavelength (LW) channel (5–42  $\mu\text{m}$ ). Its spatial resolution is 10 km for SW and 20 km for LW (from altitude 300 km). PFS uses

an onboard Fast Fourier Transform circuit to select only the data scientists are interested in [12, pp. 71, 86].

The objectives of this device are atmospheric studies like: [12, pp. 115–116]

- determining atmospheric composition (as it can detect e.g. H<sub>2</sub>O, CO and CO<sub>2</sub> spectra)
- solid-phase surface components detection
- atmospheric dust measurements
- capturing the vertical temperature–pressure profiles and dust and ice opacity

The contributions made using PFS so far are for example: [12, pp. 122–135]

- measuring the atmospheric temperature (finding out that there is a rather complicated situation around the peak of Olympus Mons)
- measuring the surface temperature
- counting the atmospheric dust content
- observing temperature inversion effects
- detecting methane in the atmosphere (which could imply either organic life or volcanic activity, which are both unexpected phenomena)
- proving that the south polar cap is made mainly from CO<sub>2</sub> ice
- capturing the solar spectrum from the surroundings of Mars (which gives results irretrievable from Earth or near Earth)

### **1.1.5 SPectroscopy for the Investigation of the Characteristics of the Atmosphere of Mars (SPICAM)**

The SPICAM instrument is made up of two spectrometers, one operating in the UV spectrum (118–320 nm) and the other in the near-IR spectrum (1.0–1.7 μm). Both these spectra provide information about (not only) H<sub>2</sub>O in the atmosphere [12, p. 95].

Many tasks have been assigned to SPICAM, the major of them being investigating ozone, H<sub>2</sub>O and aerosols vertical profiles in the atmosphere. These should help with e.g.: [12, pp. 97–100]

- constructing meteorological and dynamical atmospheric models

- understanding the water vapour atmospheric cycles
- characterizing processes of water escape from the atmosphere
- investigating the interactions between surface and atmosphere
- revealing the impact of aerosols on martian climate

One of the latest surprises brought by SPICAM is that martian atmosphere is supersaturated with water vapour which further prepares conditions for water escape from the atmosphere [24]. Another unexpected result are nocturnal aurorae observed in the upper atmosphere, along with the (expected) NO recombination nightglow [5]. Other results involve:

- retrieving global spatial and temporal climatology of ozone [29]
- south polar cap observations [20, pp. 158–159]
- studies of UV dayglow [20, pp. 160–162]
- constructing the aerosol vertical profiles [20, pp. 175–180]
- observation of CO<sub>2</sub> clouds on the nightside [20, p. 178]

### **1.1.6 Analyser of Space Plasmas and EneRgetic Atoms (ASPERA–3)**

ASPERA–3 is an instrument designed to study the interaction between solar wind and martian atmosphere. It comprises of four separate detectors. The first detector is Neutral Particle Imager (NPI) measuring the energetic neutral atom (ENA) flux with high angular resolution. Another neutral atoms sensor, the Neutral Particle Detector (NPD), measures the neutral atom flux resolving energy and mass of the atoms. The other two instruments are aimed at electrically charged particles. The Electron Spectrometer (ELS) is a top-hat electrostatic analyzer, while the Ion Mass Analyzer (IMA) is an ion mass composition analyzer working with H<sup>+</sup>, He<sup>2+</sup>, He<sup>+</sup> and O<sup>+</sup> ions [12, p. 122].

ASPERA–3 should focus on: [12, p. 122]

- measuring ENAs in order to investigate the interaction between solar wind and martian atmosphere, to characterize the impact of plasma processes on atmospheric evolution and to obtain plasma and neutral gas distribution near Mars
- measuring electrons and ions to complement ENA measurements to study the dynamics and structure of plasma and to provide solar wind parameters

To present some results of ASPERA–3 we can mention the following:

- discovering that the solar wind penetrates much deeper in martian atmosphere than was believed, being one of the atmospheric ions escape mechanisms [2]
- detection of ENA jets caused by solar wind [20, pp. 208–209]
- observing the ENA flux during Mars eclipse which laid foundation of a new method to measure planetary exosphere [20, p. 209]
- proving there is a yet unidentified source of interplanetary ENAs [20, pp. 209–212]

### 1.1.7 Mars Express Orbiter Radio Science (MaRS)

Opposite to the already described devices, the MaRS experiment does not have a dedicated physical device like a sensor or transmitter. Instead, it utilizes the antennas primarily used for communication to perform radio occultation experiments [12, p. 153]. It can use either MEX’s parabolic 1.6 m diameter High Gain Antenna or the smaller Low Gain Antennas attached to MEX. The receivers cannot be carried on board MEX, because they need to be on the opposite side of Mars than MEX is. Thus, the receivers are placed on Earth (Kourou, French Guiana; Darmstadt, Germany; Perth, Australia; three NASA’s Deep Space Network telescopes in Goldstone, USA; Madrid, Spain and Canberra, Australia). The experiment uses two frequency bands – the S-band at 2.1 GHz and the X-band at 7.1 GHz [12, pp. 153–154].

MaRS is intended to: [12, p. 141]

- sound the neutral atmosphere to derive vertical density, pressure and temperature profiles
- to sound the ionosphere (in order to get electron density profiles)
- to determine the dielectric properties of the surface
- to detect gravity anomalies
- to sound the solar corona at extra occasions

MaRS contributed to e.g.:

- improving existing atmospheric global circulation models [20, p. 227]
- discovering the so-called “meteor layer” of atmosphere containing ionized metallic atoms brought into the atmosphere by meteoric impacts [20, p. 230]
- refining the knowledge of structure and density of martian crust [20, p. 234]

### 1.1.8 Beagle 2

Beagle 2 is the lander module MEX was equipped with [12, p. 165] (its visualization is shown in Fig. 1.3). It detached from the spacecraft on 19 December 2003 (6 days before MEX orbit entry) and its touchdown was planned to 25 December 2003. However, it has not transmitted any signal after the martian atmosphere entry. As of February 2004 it was declared lost. No particular reason came out on inquiry into its fault [6].

To accomplish its main goal (searching for existing or former life, or at least for conditions allowing development of life in the past) it was equipped with the following scientific tools: [12, pp. 165–187]

- Gas Analysis Package: a mass spectrometer used for examining the surrounding atmospheric gases as well as rock and soil samples (heated in ovens in order to vaporize)
- X-Ray Spectrometer: used for studying the composition of rock and soil samples using X-Ray fluorescence spectrometry being able to detect metals like Fe, Mg, Al, Ti and others
- Mössbauer Spectrometer: designed to analyze materials containing iron
- Stereo Camera System: intended for acquiring stereoscopic images of the landing site in various spectral ranges
- Microscopic Imager: should have provided one of the largest contributions to Beagle's main goal (by searching for microscopic fossils)
- Planetary Underground Tool: developed as a support for all the mentioned systems; it should have obtained soil samples using a 1.5 m long drill
- there is also a grinder available for removing unwanted material from the samples or the surrounding surface

There were also several sensors attached to Beagle 2: [12, pp. 188–191]

- the oxidant sensor monitoring the oxidizing effects of martian atmosphere
- the UV sensor capturing the UVA and UVB spectral ranges (which are lethal for organisms)
- the wind sensor recording the speed and direction of wind
- the air pressure sensor with resolution 0.003 hPa
- the air temperature sensor with accuracy about 0.01 K
- the dust impact monitor measuring the magnitude and impact rate of dust particles



Figure 1.3: Visualization of the Beagle 2 lander on martian surface. [3]

## 1.2 The MARSIS experiment

In this section, we discuss the individual parts of the MARSIS experiment. We briefly describe the physical background of the experiments as well as the technical solution of the measurement mechanisms.

### 1.2.1 Subsurface sounding

The subsurface sounding attempts to detect the borders of the cryosphere, which is the crust layer in which the temperature remains constantly under the water-freezing point. Such borders can be identified owing to different dielectric properties of liquid water, ice and atmospheric gases. The deeper border can be a water–ice interface. This is because the cryosphere ends at the depth where the internal planetary heat flow raises the temperature above the water-melting point. So if there is a liquid water reservoir under the cryosphere, it can be detected. This interface is expected to be at 0–5,000 m depth. On the other hand, the higher border can be formed by the desiccated megaregolith (martian soil) where the desiccation is caused by subsurface ice sublimation (estimated to be at depths between 0 and 1,000 m) [12, pp. 52–53].

As described in part 1.1.3, MARSIS can utilize a 40 m long dipole antenna as well as a 7 m monopole one. Only the dipole antenna is used for signal transmission (generating up to 10 W strong signal), and both antennas for signal

receipt. It can sound using one of the four subsurface frequency bands centered at 1.8, 3, 4 and 5 MHz, every one having 1 MHz bandwidth. When MEX operates on the dayside of Mars, the ionosphere does not allow to use lower frequency bands for sounding (see section 1.2.3), so only the last two bands can be used. On the nightside, all four bands get through the ionosphere and allow to sound deeper subsurface. However, due to the limitations given by the MEX spacecraft, only echoes from depths up to 5–8 km can be detected [12, p. 57].

The subsurface sounder mode is based on the fact that the radar waves reflect not only on the surface, but also on subsurface dielectric discontinuities. In addition, the velocity of the waves decreases proportionally to the material loss tangent, the wavelength and the depth – which facilitates computing the depth of subsurface interfaces [12, p. 56].

### 1.2.2 Surface sounding

It arises from the previous paragraphs that the surface sounding mode is a “subset” of the subsurface sounding mode, taking only the “topmost” echoes into account. Therefore, no additional operation modes are present for just the surface sounding.

The surface sounding is used to create a topography of the surface with lateral resolution 5–9 km. This topography further serves for improving the accuracy of statistical topography models which describe the surface in the means of a random distribution of heights [12, p. 54].

### 1.2.3 Ionospheric sounding

The basic reason for studying the ionosphere is that it stops propagation of electromagnetic waves with frequencies below the local electron plasma frequency  $f_p$ . This frequency can be expressed as  $f_p = 8980\sqrt{N_e}$  Hz, where  $N_e$  is the local electron density in  $\text{cm}^{-3}$ . All vertical waves with frequencies below the maximum electron plasma frequency,  $f_p(\text{max})$ , are reflected back at a height with the same frequency as the waves have. This maximum is usually located at the heights 125–150 km and amounts up to 4 MHz on the dayside and 800 kHz on the nightside [12, pp. 55–56].

MARSIS uses two methods – a passive and an active one. The passive method measures thermal emission at the local electron plasma frequency. The active method – the one of our interest – sounds the ionosphere with the radar in 160 frequency steps ranging from 100 kHz to 5.4 MHz. With such sampling it is possible to construct vertical profiles of the electron plasma frequency (and also electron density). Besides the normal ionospheric sounding mode, MARSIS also provides a special interleaved mode switching periodically between the subsurface

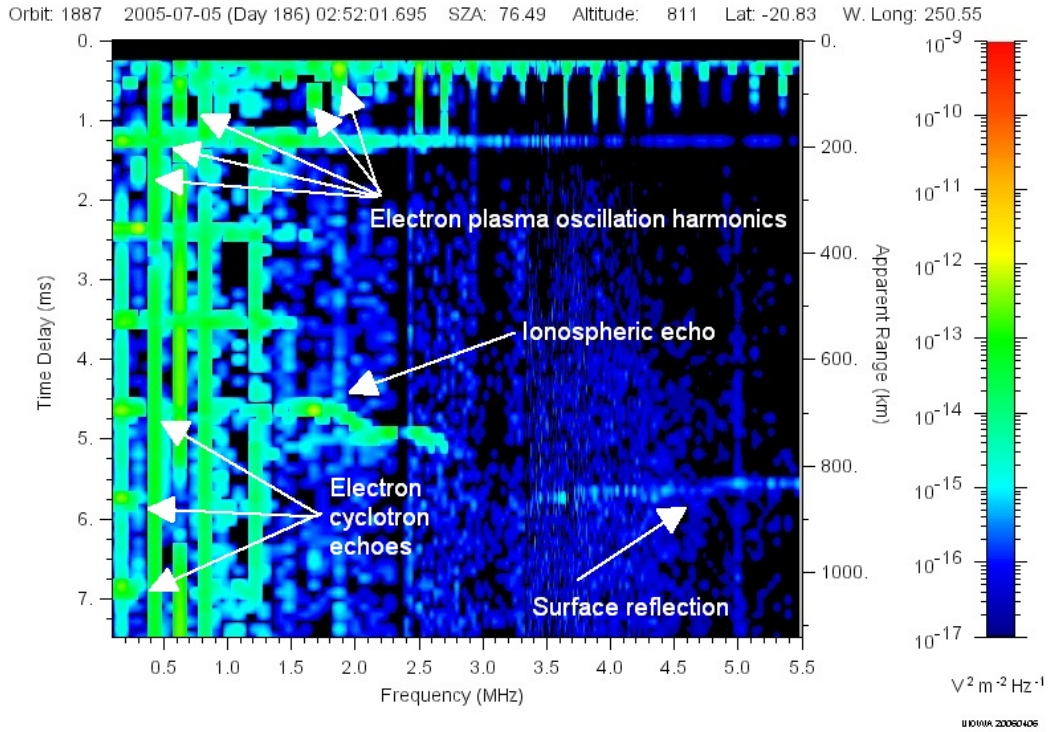


Figure 1.4: Example of a ionogram showing most of the detectable features like ionospheric echo, surface reflection, electron cyclotron echoes and electron plasma oscillation harmonics. No oblique ionospheric echo is present. The vertical axis shows delay time in ms, the horizontal axis stands for frequency in MHz and color codes the spectral density of the received electric field in  $\text{V}^2 \text{m}^{-2} \text{Hz}^{-1}$ . Based on real data obtained from [8].

sounding and ionosphere sounding modes. This yields a method to remove the ionospheric effects from the subsurface sounding results [12, p. 58].

Adding to the ionospheric and surface echoes, there are three more (unexpected [21, p. 1930], but useful) signal patterns detectable using the ionospheric sounding. Namely, oblique ionospheric echoes, electron plasma oscillation harmonics and electron cyclotron echoes. We will describe all of them in the following sections after presenting the concept of ionograms.

### 1.3 Ionograms

Ionograms are the basic visualization of the ionospheric sounding data. Akalin [1] defines ionograms in the following precise way:

Ionograms are produced by transmitting a short pulse at a fixed frequency,  $f$ , and measuring the received intensity at 80 consecutive values of the time delay,  $\Delta t$ , spaced  $91.4 \mu\text{s}$  apart. The frequency is then incremented and the process is repeated. For each of the

160 frequencies, quasi-logarithmically ( $\Delta f/f \approx 2\%$ ) spaced between 0.1 and 5.5 MHz, there are 80 delay time bins spaced 91.4  $\mu$ s apart. The bins start 162.5  $\mu$ s after the end of the sounding pulse. This gives 7.32 ms per one frequency and 1.26 s overall for the 160 frequencies (there is a small delay between the steps). Such complex sounding scan can be repeated every 7.54 s. Ionograms represent received intensity as a function of time delay and frequency. As shown by the ionogram in Fig. 1.4, time delay is displayed in milliseconds along the vertical axis, frequency is displayed in megahertz along the horizontal axis, and the color bar represents the received electric field spectral density in  $V^2 m^{-2} Hz^{-1}$ .

Several more or less continuous patterns can be found in the example ionogram. Some of them form repetitious patterns. It can be also seen that the data are very noisy. The example ionogram is rather rare, because often just one or two such patterns occur in a single ionogram. There are also ionograms consisting entirely of noise. The subsequent sections will discuss all the patterns and their physical meaning.

### 1.3.1 Ionospheric echo

As seen in Fig. 1.4, the ionospheric echo is a horizontally oriented non-straight line. It usually appears in the lower half of the ionogram (delay times about 4 to 5 ms). Under ideal conditions, its left end should start at the local electron plasma frequency, which is most often somewhere below 1 MHz. However, in practice the emitted power is too low at low frequencies and the echo vanishes in noise. Its right end should be placed at  $f_p(\max)$  frequency, where all higher-frequency waves pass to the surface [21, p. 1929].

There is often a sharp cusp at the right end of the echo. “The cusp occurs because the propagation speed of the wave packet (i.e., the group velocity) is very small over an increasingly long path length as the wave frequency approaches  $f_p(\max)$ ” [21, p. 1929]. On the other hand, the echo often does not extend up to  $f_p(\max)$  [21, p. 1930].

As we have mentioned earlier, it is possible to compute the local electron plasma frequency from the echo’s delay time, thus obtaining the electron density vertical profile. In order to extract the profile, it is needed to identify the curve fitting the echo. Automatic identification of such curve is one of the goals of this work. Especially correct estimation of the right end would be helpful if the cusp is present.

### 1.3.2 Surface echo

Similar to the ionospheric echo is the surface echo. It is placed lower than the ionospheric echo (because the ionosphere is closer to the sounder than surface is). Its left end is at the same frequency where the ionospheric echo's right end should be, i.e. at the  $f_p(\max)$  frequency. It should extend up to the right edge of the ionogram (since all frequencies higher than  $f_p(\max)$  penetrate the ionosphere) [21, p. 1929].

The same (but mirrored) cusp as in ionospheric echo should be present at the left end of the surface echo, caused by the same effect.

It is common that there is no surface echo in the ionogram. It can have several reasons. One of them is that the surface absorption of the radar waves increases with decreasing solar zenith angle (at angles lower than  $40^\circ$  the surface echoes are rare). Another way to stop the waves from returning to the sounder could be charged particles from solar flares ionizing the lower levels of ionosphere [21, p. 1930].

From surface echoes it is easy to read the apparent height over surface (omitting the cusp area). However, due to the frequent problems with absorption and low spatial resolution it is not a practically useful for topography. At least, the surface-caused attenuation of the signal can be derived from the echo.

### 1.3.3 Oblique ionospheric echo

The first of unexpected features emergent in ionograms are oblique ionospheric echoes. An example of such echo is displayed in Fig. 1.5. It is an echo of similar shape and horizontal boundaries as the ionospheric echo, but located a few ms lower in the ionogram. Often even lower than the surface echo – but the radar waves do not even reach the surface at the frequencies of the ionospheric echo.

An explanation of this effect is given in [21, pp. 1931–1933]. At locations with strong crustal magnetic field, this field forms bulges in the ionosphere. Such bulges, if lying aside the MEX track, reflect the waves from the sounder under such angle that the antenna records the reflections. However, since the track of these waves is not vertical, they may travel longer distances than to the surface before they return. An illustration of this effect is provided in Fig. 1.6.

To detect oblique echoes in ionograms could be of some use, because they point to places with ionosphere bulges and strong crustal fields. However, deriving the shapes of the bulges or the crustal fields would be very complicated [21, p. 1932]. Therefore, we will not try to detect them in the task-specific algorithms devised in this thesis.

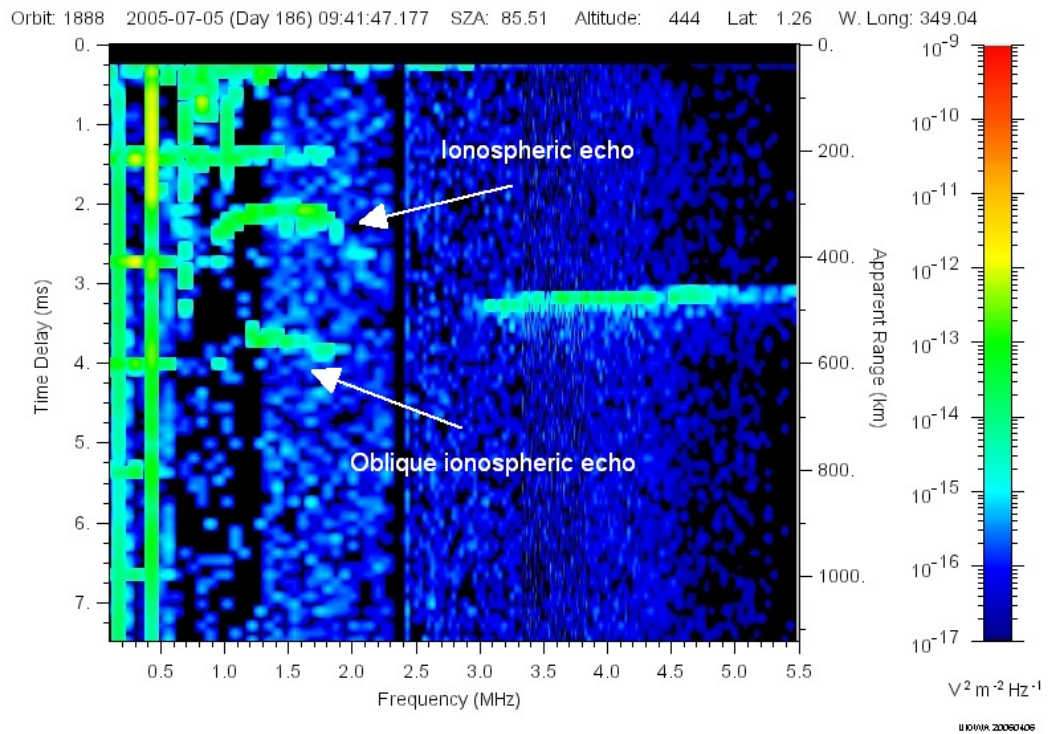


Figure 1.5: A ionogram containing oblique ionospheric echo. It is worth notice that the echo appears to origin under the surface level (because of the delay time higher than the delay time to surface). Based on real data obtained from [8].

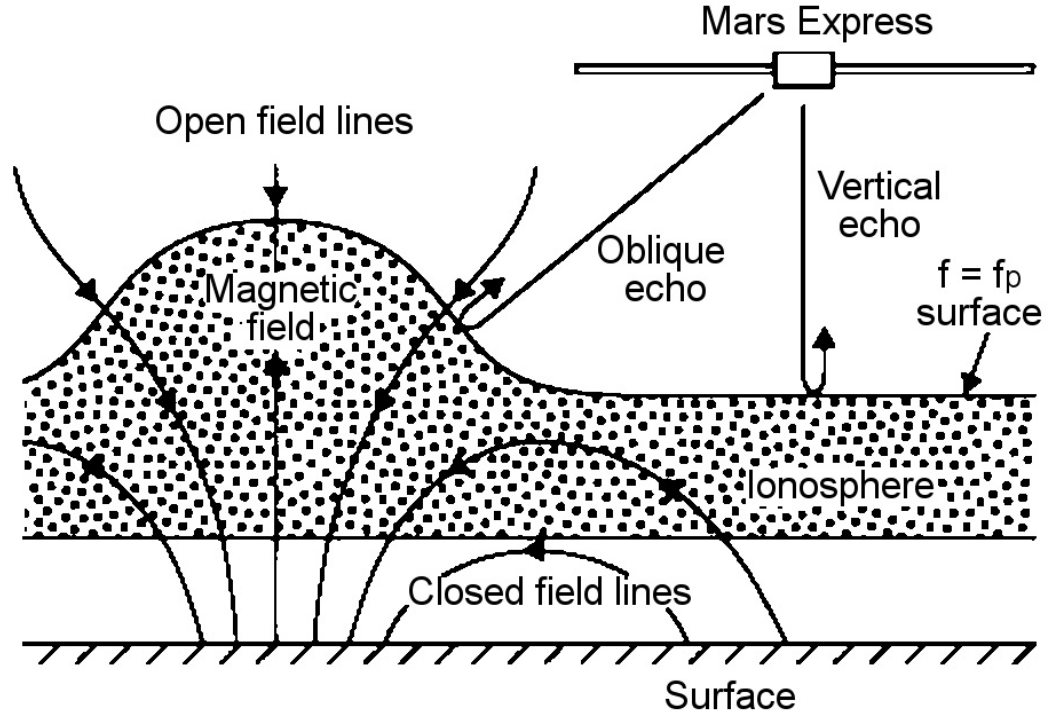


Figure 1.6: A ionospheric bulge created by strong crustal magnetic field can produce oblique ionospheric echoes. [21]

### 1.3.4 Electron plasma oscillation harmonics

Another surprise are repetitious straight vertical lines in ionograms, electron plasma oscillation harmonics (called also Langmuir waves [11, p. 2]). As can be seen in Fig. 1.4, they appear near the top left corner of ionograms. They always start at the top of the image and continue towards the bottom; they may disappear on any time delay. Although they are mainly located in the left part of ionograms, occasionally they may repeat up to the right edge. More than 10 repetitions are, however, rare [11, p. 4].

It is stated in [21, p. 1929] that these echoes “are at harmonics of the local electron plasma frequency and are caused by the excitation of electron plasma oscillations, [...]. Even if the fundamental of the plasma frequency is not observed directly [...], the plasma frequency can still be determined from the spacing of the harmonics.” The reason why not only the base frequency is present, but also its harmonics, is described in [11, p. 2]: “Since the electron plasma oscillations are usually very intense, [...] the received waveforms are often severely clipped. The resulting distortion then introduces harmonics at multiples of the basic oscillation frequency.”

As all features detected by the ionospheric sounder, also plasma oscillation harmonics may not be present in a ionogram. There are three main reasons for it: when the local electron density is less than  $10 \text{ cm}^{-3}$ , when the plasma flow velocity is more than  $160 \text{ km/h}$  or when the temperature is greater than  $8,521 n_e \text{ K}$  ( $n_e$  stands for electron density in  $\text{cm}^{-3}$ ; this happens in solar wind) [11, p. 4].

Although the base oscillation frequency is occasionally captured in ionograms (when higher than  $100 \text{ kHz}$ , the sounder’s lowest frequency), it is apparently more precise to derive the frequency from the harmonics spacing (using multiple fit). That is what we will focus on in later chapters.

As a benefit, this method allows to measure the electron density down to  $10 \text{ cm}^{-3}$  which corresponds to heights up to  $1,300 \text{ km}$ . Such low densities could not be detected by the radar sounder.

### 1.3.5 Electron cyclotron echoes

The last unanticipated phenomenon appearing in ionograms are the electron cyclotron echoes. These are regularly-repeating straight horizontal lines in ionograms. They always start from the lowest sounding frequency (the left edge) and extend to frequencies up to  $2 \text{ MHz}$  [1, p. 3]. It can be observed in Fig. 1.4 that the repetition can appear at the whole vertical range.

Comparing with the magnetic field model of Mars, Gurnett [21] determined that the repetition frequency of these echoes corresponds to local electron

cyclotron frequency  $f_c$ . That frequency can be expressed as  $f_c = 28 B$  Hz,  $B$  being the magnetic field strength in nT. Thus, knowing the repetition rate of the echoes, we are able to determine the strength of the magnetic field. That is a very important application, since MEX does not carry a magnetometer [21, p. 1930]. There is also a method to derive the vector component of the magnetic field under some conditions [1].

The origin of these echoes is described in [21, p. 1930]: “We believe that these echoes are caused by electrons accelerated by the strong electric fields near the antenna during each cycle of the transmitter waveform. The cyclotron motion of the electrons in the local magnetic field then causes these electrons to periodically return to the vicinity of the antenna, where they induce a signal on the antenna.”

Some constraints, of course, apply to the presence of cyclotron echoes in ionograms. Firstly, the magnetic field strength must be uniform on an area larger than the cyclotron radius (which is about 1 km). According to [21, p. 1930] this is easily satisfied. Further, the sounder’s minimum and maximum time delay resolution constrains the detectable field strengths. The minimum resolution of 182.2  $\mu$ s corresponds to field strength of 195 nT, while the maximum delay of 7.5 ms corresponds to field strength of about 5 nT. However, in practice the reasonable range for confident measurements is about 12 – 160 nT [1, p. 3].

Similarly to the plasma oscillation harmonics, we are interested in the period of repetition of these echoes. If we can compute it, we are able to compute the strength of the magnetic field and, in some cases, also its direction. We will also focus on detection of this period in our survey.

# 2 The detection problem

In the previous chapter, we have presented the physical background of ionograms. We have also shown the four major features that can be detected in them. In this part we try to make a transition to the technical point of view. Firstly we define the problem in the context of computer vision.

## 2.1 Definition

Now we are to seek for definitions of the basic terms used throughout the rest of this work. In order to precisely define the detection problem, we need to know the definitions of what a ionogram or its feature is. We also specify what attributes should a detection result have. Finally, we introduce some measures of quality of the detection.

### 2.1.1 Ionogram

As stated in section 1.3, a ionogram consists of electric field density measured at 160 frequencies and within 80 consequent time steps. Thus, we can treat a ionogram as a real-valued image (or a two-dimensional array) of dimension 160x80. The range of values at each pixel is  $10^{-24}$  to  $10^{-10} \text{ V}^2\text{m}^{-2}\text{Hz}^{-1}$  (we haven't found an authoritative source for this information, but instead we deduced it from a large set of ionograms). However, values lower than  $10^{-17}$  are considered to be background, so we can treat them as zeros. The horizontal indices are interpreted as the sounding frequency and they come from the range 0.1 – 5.5 MHz. The mapping from indices to frequencies is nonuniform and may differ for individual ionograms (it depends on the used frequency table; but a single table is preferred in most of the data). Every ionogram carries information about this mapping with it. On the other hand, the vertical indices map always to the same uniformly distributed values. They start at 162.5  $\mu\text{s}$  and go up to 7.32 ms using steps of height 91.4  $\mu\text{s}$  (assuming the lowest value to be at top).

As we are going to detect repetitious features, the ionogram with unevenly distributed frequency assignment would be impractical. To overcome this, we introduce the notion of “evenly sampled ionogram”. To get an evenly sampled ionogram from a normal ionogram, we first extend each frequency column so that we will be able to map all the new columns to a linear axis. The new width of the ionogram should be at least the frequency range (5.4 MHz) divided by the frequency width of the narrowest column (in order to allow every new column to have its width at least 1 px). We also stretch rows by the same amount to preserve aspect ratio. Next we interpolate the new columns using

linear interpolation. If column  $i$  stretched to columns  $j \dots j+k$ , the values at column  $j$  are copied and for every column  $c \in <j+1; j+k>$  the value will be  $v[c] = v[j] * (1 - \frac{c-j}{k}) + v[j+k+1] * \frac{c-j}{k}$  (where  $v[c]$  denotes the vector of values at column  $c$ ). Then we perform the same interpolation vertically to fill missing values in columns. This interpolation of course doesn't add any new information to the image, but it allows us to work on an image with both axes in uniform linear scale. Any other kind of interpolation of missing pixels can be used as long as it preserves the values corresponding to the "original pixels". The difference between normal and evenly sampled ionogram is shown in Fig. 2.1.

### 2.1.2 Features to detect

We have listed four features of interest - ionospheric echoes (IE), ground echoes (GE), electron plasma oscillations (EPO) and electron cyclotron harmonics (ECH) (in section 1.3.3 we have already stated we will omit oblique ionospheric echoes). We detect them based on the fact that they correspond to areas with significantly higher ionogram values than the background. However, ionograms are often very noisy, so it would be difficult (if not impossible) to define a single absolute threshold for telling whether a pixel belongs to a feature or not.

For verification purposes we manually tagged 115,495 ionograms from 1,014 orbits during year 2007. In most of these ionograms we measured the horizontal repeat period (corresponding to EPO) and marked the ionospheric echoes. If no horizontal repetition period was present, we recorded that fact, too. Although being done manually and thus each feature being assessed subjectively, we deduced a rule for distinguishing interesting lines (which are either a feature or a part of a feature). Such line is several pixels wide (cca. 3–20 px) and at least that much pixels long (assuming the ionogram has dimension 1,012x506 px). Values on its skeleton (center line) are at least 10 times higher than those at its border. A line is also allowed to contain "gaps", but no more than a third of the line's length in sum. Moreover, every line should contain a value higher than cca.  $5 \times 10^{-15}$  (but not all points with higher values belong to a feature). Such definition looks, however, vague. So we add other specific constraints implying from the features we try to detect.

An EPO or ECH line must be almost straight and must go in exactly vertical or horizontal direction. In addition, one of its ends has to be near the top or left edge of the ionogram (no more than 5 px). ECH lines usually do not extend to frequencies above 2.5 MHz. A GE line follows approximately horizontal direction and doesn't have to be straight (due to terrain unevenness; but mostly it is). What should be most helpful is it is placed in the delay time corresponding to the apparent height of the spacecraft over surface (which can be computed). Finally, an IE line has also to be almost horizontal, but it may be substantially

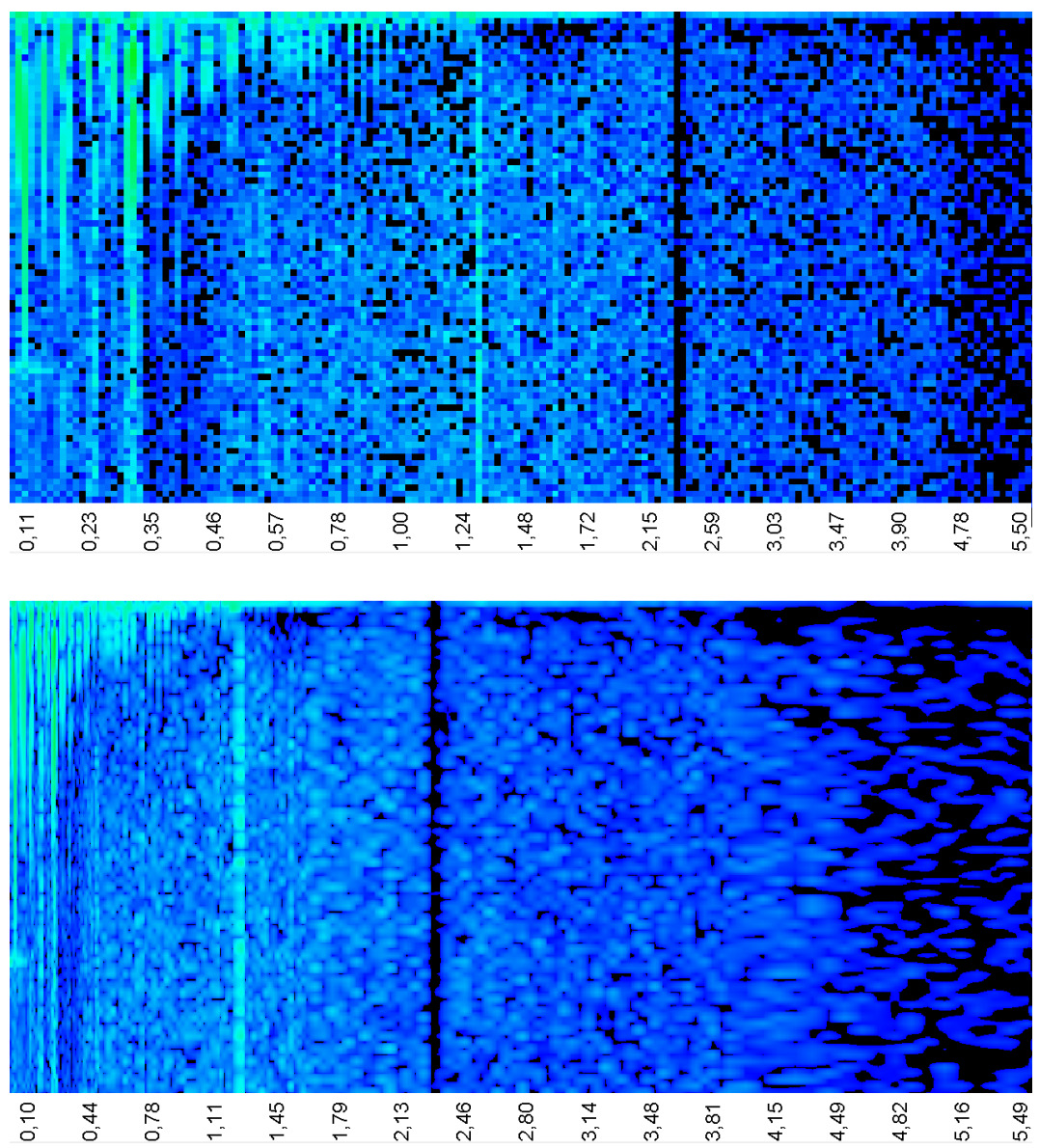


Figure 2.1: In the top part of this figure, a ionogram is presented. In the bottom part, an evenly sampled ionogram created from the top one is presented. It is worth notice that the labels of horizontal (frequency) aces of the top ionogram are unevenly distributed. Data from orbit 3874, frame 0 [8].

curved. It has to appear over the GE (if present).

The statistical tests we conducted<sup>1</sup> on the data from year 2007 show that 95 % ionograms with some features have their mean value greater than  $4.653,12 \times 10^{-16}$ . Ionograms devoid of features have, of course, their mean values even lower than this value (in 74.6 % of cases). So we decided this value to be a threshold for telling a ionogram does not contain any features and we will not process it further. This is useful, because the detection algorithms can assume the ionogram either has some features or isn't far from having them.

We also computed other statistical properties of ionograms. We expected the maximum values in ionograms to be a reliable distinguishing mark, and standard deviations, too. As shown in Fig. 2.2, neither maxima nor standard deviations show significant differences between the data sets with features and without them. We also made distributions of rather high values (over  $10^{-12}$ ) in relation to whether they are a part of a feature. The results shown almost identical distributions, but that can be due to the difficulty of reverse task. E.g. if we save just the period of an EPO, it isn't easily said if a data point belongs to this feature (we try to fit it on whole multiplies of the period, but we don't know the widths of the lines).

## 2.2 Title of the second subchapter of the second chapter

---

<sup>1</sup>The application used for these tests is present on the attached CD in folder /programs/statistics along with the data.

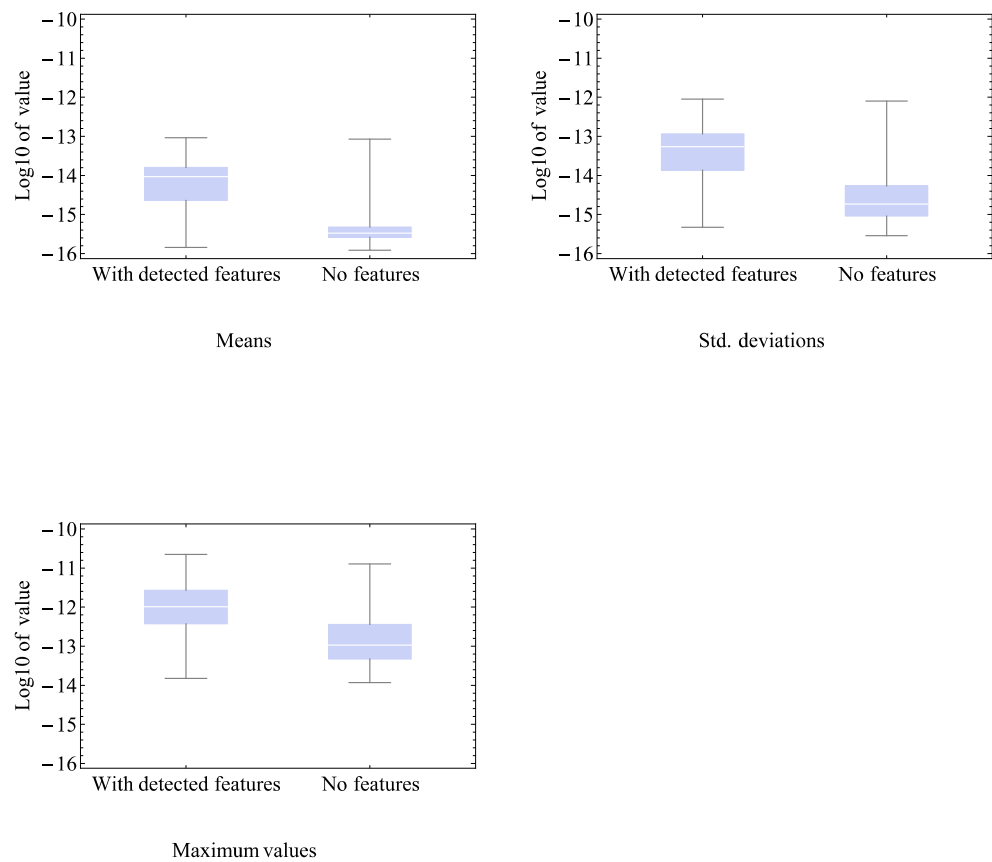


Figure 2.2: The distribution of means (top left), standard deviations (top right) and maximum values (bottom left) of individual ionograms from year 2007. The box plots show values for ionograms with features and without features separately. Data from [8].

# Conclusion

# Bibliography

- [1] AKALIN, F. et al. Dayside induced magnetic field in the ionosphere of Mars. *Icarus*. March 2010, 206, 1, pages 104–111. ISSN 00191035. doi: 10.1016/j.icarus.2009.03.021. Available from: <http://linkinghub.elsevier.com/retrieve/pii/S0019103509001316>.
- [2] BARABASH, S. et al. Martian atmospheric erosion rates. *Science (New York, N.Y.)*. January 2007, 315, 5811, pages 501–3. ISSN 1095-9203. doi: 10.1126/science.1134358. Available from: <http://www.ncbi.nlm.nih.gov/pubmed/17255508>.
- [3] BEAGLE\_2. *Beagle 2 lander*. In *Space In Images* [online], 2002. [Accessed 03/24/2013]. Available from: [http://spaceinimages.esa.int/Images/2001/11/Beagle\\_2\\_lander](http://spaceinimages.esa.int/Images/2001/11/Beagle_2_lander).
- [4] BERTAUX, J. L. et al. First detection of O<sub>2</sub> 1.27 μm nightglow emission at Mars with OMEGA/MEX and comparison with general circulation model predictions. *Journal of Geophysical Research*. March 2012, 117, pages E00J04. ISSN 0148-0227. doi: 10.1029/2011JE003890. Available from: <http://www.agu.org/pubs/crossref/2012/2011JE003890.shtml>.
- [5] BERTAUX, J.-L. et al. Nightglow in the upper atmosphere of Mars and implications for atmospheric transport. *Science (New York, N.Y.)*. January 2005, 307, 5709, pages 566–9. ISSN 1095-9203. doi: 10.1126/science.1106957. Available from: <http://www.ncbi.nlm.nih.gov/pubmed/15681381>.
- [6] BONACINA, F. *Lessons Learnt From Beagle 2 And Plans To Implement Recommendations From The Commission Of Inquiry*. In *Ireland / ESA in your country* [online], 2004. [Accessed 03/24/2013]. Available from: [http://www.esa.int/ESA\\_in\\_your\\_country/Ireland/Lessons\\_learnt\\_from\\_Beagle\\_2\\_and\\_plans\\_to\\_implement\\_recommendations\\_from\\_the\\_Commission\\_of\\_Inquiry](http://www.esa.int/ESA_in_your_country/Ireland/Lessons_learnt_from_Beagle_2_and_plans_to_implement_recommendations_from_the_Commission_of_Inquiry).
- [7] CHEVRIER, V., POULET, F., BIBRING, J.-P. Early geochemical environment of Mars as determined from thermodynamics of phyllosilicates. *Nature*. July 2007, 448, 7149, pages 60–3. ISSN 1476-4687. doi: 10.1038/nature05961. Available from: <http://www.ncbi.nlm.nih.gov/pubmed/17611538>.
- [8] CHICARRO, A. *MEX MARSIS AIS data*. In *Planetary Science Archive* [online], 2005. [Accessed 03/26/2013]. Available from: <ftp://psa.esac.esa.int/pub/mirror/MARS-EXPRESS/MARSIS>.

- [9] CLARK, S. *Mars Express back in business at the red planet*. In *Spaceflight Now* [online], 2012. [Accessed 03/20/2013]. Available from: <http://www.spaceflightnow.com/news/n1202/15marsexpress/>.
- [10] DOUTÉ, S. et al. South Pole of Mars: Nature and composition of the icy terrains from Mars Express OMEGA observations. *Planetary and Space Science*. January 2007, 55, 1-2, pages 113–133. ISSN 00320633. doi: 10.1016/j.pss.2006.05.035. Available from: <http://linkinghub.elsevier.com/retrieve/pii/S0032063306001243>.
- [11] DURU, F. et al. Electron densities in the upper ionosphere of Mars from the excitation of electron plasma oscillations. *Journal of Geophysical Research*. 2008, 113, A7, pages A07302. ISSN 0148-0227. doi: 10.1029/2008JA013073. Available from: <http://www.agu.org/pubs/crossref/2008/2008JA013073.shtml>.
- [12] ESA. *Mars Express: the scientific payload*. Noordwijk, Netherlands: ESA Publications Division, 2004. Available from: [www.esa.int/esapub/sp/sp1240/sp1240web.pdf](http://www.esa.int/esapub/sp/sp1240/sp1240web.pdf). ISBN 92-9092-556-6.
- [13] ESA. Mars Express Master Science Plan Part I - Introduction. Technical Report 1, 2004. Available from: <http://www.rssd.esa.int/SB/MARSEXPRESS/docs/MSPDOC/MSPOverviewDocumentation-PartI.pdf>.
- [14] ESA. *Mars Express Radar Deployment Postponed*. In *ESA Science & Technology* [online], 2004. [Accessed 03/20/2013]. Available from: <http://sci.esa.int/science-e/www/object/index.cfm?fobjectid=35021>.
- [15] ESA. *Mars Express 2nd Boom Deployed*. In *ESA Science & Technology* [online], 2005. [Accessed 03/20/2013]. Available from: <http://sci.esa.int/science-e/www/object/index.cfm?fobjectid=37608>.
- [16] ESA. *Mars Express and the mystery of Phobos*. In *ESA Kids Liftoff* [online], 2010. [Accessed 20. 3. 2013]. Available from: [http://www.esa.int/esaKIDS/SEM8534KV5G\\_Liftoff\\_1.html](http://www.esa.int/esaKIDS/SEM8534KV5G_Liftoff_1.html).
- [17] ESA. *Mars Express steadily returns to routine operation*. In *ESA Our Activities* [online], 2011. [Accessed 03/20/2013]. Available from: [http://www.esa.int/Our\\_Activities/Operations/Mars\\_Express\\_steadily\\_returns\\_to\\_routine\\_operation](http://www.esa.int/Our_Activities/Operations/Mars_Express_steadily_returns_to_routine_operation).
- [18] ESA. Programmes in Progress. *Bulletin Space for Europe issue 148*. 2011, pages 72–73. Available from: <http://esamultimedia.esa.int/multimedia/publications/ESA-Bulletin-148/pageflip.html>.

- [19] ESA. *Fact Sheet*. In *ESA Science & Technology* [online], 2013. [Accessed 03/20/2013]. Available from: <http://sci.esa.int/science-e/www/object/index.cfm?fobjectid=47364>.
- [20] FLETCHER, K., WITASSE, O. *MARS EXPRESS: The Scientific Investigations*. Noordwijk, Netherlands: ESA Communication Production Office ESTEC, 2009. Available from: <http://sci.esa.int/science-e/www/object/index.cfm?fobjectid=47218>. ISBN 978-92-9221-975-8.
- [21] GURNETT, D. a. et al. Radar soundings of the ionosphere of Mars. *Science (New York, N.Y.)*. December 2005, 310, 5756, pages 1929–33. ISSN 1095-9203. doi: 10.1126/science.1121868. Available from: <http://www.ncbi.nlm.nih.gov/pubmed/16319123>.
- [22] JAUMANN, R. et al. The high-resolution stereo camera (HRSC) experiment on Mars Express: Instrument aspects and experiment conduct from interplanetary cruise through the nominal mission. *Planetary and Space Science*. May 2007, 55, 7-8, pages 928–952. ISSN 00320633. doi: 10.1016/j.pss.2006.12.003. Available from: <http://linkinghub.elsevier.com/retrieve/pii/S0032063306003448>.
- [23] LOIZEAU, D. et al. Characterization of hydrated silicate-bearing outcrops in Tyrrhena Terra, Mars: Implications to the alteration history of Mars. *Icarus*. May 2012, 219, 1, pages 476–497. ISSN 00191035. doi: 10.1016/j.icarus.2012.03.017. Available from: <http://linkinghub.elsevier.com/retrieve/pii/S0019103512001108>.
- [24] MALTAGLIATI, L. et al. Evidence of water vapor in excess of saturation in the atmosphere of Mars. *Science (New York, N.Y.)*. September 2011, 333, 6051, pages 1868–71. ISSN 1095-9203. doi: 10.1126/science.1207957. Available from: <http://www.ncbi.nlm.nih.gov/pubmed/21960630>.
- [25] MANGOLD, N. et al. Geomorphic study of fluvial landforms on the northern Valles Marineris plateau, Mars. *Journal of Geophysical Research*. August 2008, 113, E8, pages E08009. ISSN 0148-0227. doi: 10.1029/2007JE002985. Available from: <http://www.agu.org/pubs/crossref/2008/2007JE002985.shtml>.
- [26] MASSÉ, M. et al. Mineralogical composition, structure, morphology, and geological history of Aram Chaos crater fill on Mars derived from OMEGA Mars Express data. *Journal of Geophysical Research*. December 2008, 113, E12, pages E12006. ISSN 0148-0227. doi: 10.1029/2008JE003131. Available from: <http://www.agu.org/pubs/crossref/2008/2008JE003131.shtml>.

- [27] MONTMESSIN, F. et al. Hyperspectral imaging of convective CO<sub>2</sub> ice clouds in the equatorial mesosphere of Mars. *Journal of Geophysical Research*. November 2007, 112, E11, pages E11S90. ISSN 0148-0227. doi: 10.1029/2007JE002944. Available from: <http://www.agu.org/pubs/crossref/2007/2007JE002944.shtml>.
- [28] NEUKUM, G. *Amenthes Planum topography*. In *Space In Images* [online], 2013. [Accessed 03/21/2013]. Available from: [http://spaceinimages.esa.int/Images/2013/02/Amenthes\\_Planum\\_topography](http://spaceinimages.esa.int/Images/2013/02/Amenthes_Planum_topography).
- [29] PERRIER, S. et al. Global distribution of total ozone on Mars from SPICAM/MEX UV measurements. *Journal of Geophysical Research*. 2006, 111, E9, pages E09S06. ISSN 0148-0227. doi: 10.1029/2006JE002681. Available from: <http://www.agu.org/pubs/crossref/2006/2006JE002681.shtml>.
- [30] PHILLIPS, R. J. et al. Mars north polar deposits: stratigraphy, age, and geodynamical response. *Science (New York, N.Y.)*. May 2008, 320, 5880, pages 1182–5. ISSN 1095-9203. doi: 10.1126/science.1157546. Available from: <http://www.ncbi.nlm.nih.gov/pubmed/18483402>.

# List of Tables

# List of Abbreviations

# Attachments